# Combined Effects of Functional Groups, Lattice Defects, and Edges in the Infrared Spectra of Graphene Oxide

Cui Zhang,[†] Daniel M. Dabbs,[‡] Li-Min Liu,[†,§] Ilhan A. Aksay,[‡] Roberto Car,[†] and Annabella Selloni[*,†]

[†]Department of Chemistry and [‡]Department of Chemical and Biological Engineering, Princeton University, Princeton, New Jersey 08544, United States

S *Supporting Information*
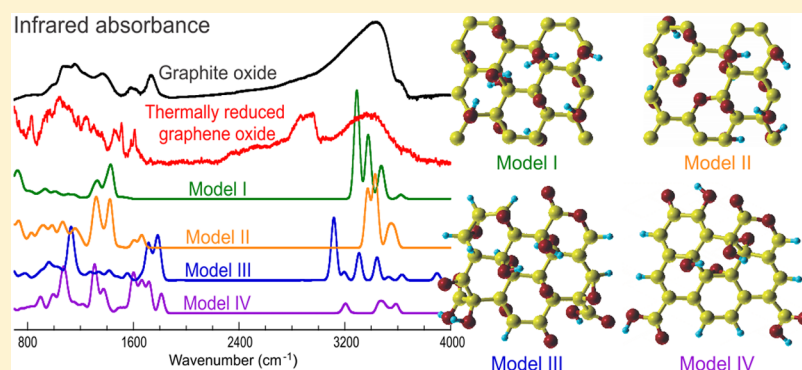
ABSTRACT: Infrared spectroscopy in combination with density functional theory calculations has been widely used to characterize the structure of graphene oxide and its reduced forms. Yet, the synergistic effects of different functional groups, lattice defects, and edges on the vibrational spectra are not well understood. Here, we report first-principles calculations of the infrared spectra of graphene oxide performed on realistic, thermally equilibrated, structural models that incorporate lattice vacancies and edges along with various oxygen-containing functional groups. Models including adsorbed water are examined as well. Our results show that lattice vacancies lead to important blue and red shifts in the OH stretching and bending bands, respectively, whereas the presence of adsorbed water leaves these shifts largely unaffected. We also find unique infrared features for edge carboxyls resulting from interactions with both nearby functional groups and the graphene lattice. Comparison of the computed vibrational properties to our experiments clarifies the origin of several observed features and provides evidence that defects and edges are essential for characterizing and interpreting the infrared spectrum of graphene oxide.

INTRODUCTION

Graphene oxide and its reduced forms have attracted significant attention in recent years. Graphene oxide, with a carbon-to-oxygen atomic ratio (C/O) of around 2,[1,2] was first studied by Hwa et al. in 1991 as a two-dimensional macromolecule.[3] Fully oxidized graphene can reach a C/O of ∼ 1.3.[4,5] While the high oxygen content makes graphene oxide an insulator, it can be converted to an electrically conducting state by increasing its C/O above ∼ 6[6] using thermal[6−10] or chemical[11,12] reduction methods. Reduced graphene oxides, which we refer to as functionalized graphene sheets (FGSs),[6,9] have demonstrated promising performance in many applications, including fuel cells,[13,14] propellants,[15,16] structural composites,[17−19] super-capacitors,[13,20] batteries,[21−23] electrochemical sensors,[24−26] and dye-sensitized solar cells.[27,28]

The increasing interest and application of FGSs spurred the development of a process now used for the large-volume fabrication of FGSs.[29] Briefly, the process involves three steps: (i) producing graphite oxide (GO) by oxidizing graphite, (ii) thermally exfoliating and partially reducing the GO to form the FGSs, and (iii) additional thermal reduction of the FGS to

set the C/O.[6,9,29] For example, to fabricate FGS with a C/O near 100, GO is produced using a modified Hummers method,[11] which is then simultaneously exfoliated and reduced to form FGSs with C/O near 10.[6,7,9] The targeted C/O of 100 is achieved by thermally reducing the FGS at 1100 °C under argon for 1 h.[8] In Figure 1, we show the spectra from diffuse reflectance infrared Fourier transform spectroscopy (DRIFTS) performed on GO and heat-treated FGS prepared in the described manner.

Models of the structure of graphene oxide based on density functional theory (DFT)[6,9,30−40] have been used to generate tables of functional group IR absorption band assignments for graphene oxide and its derivatives (see Tables S1 and S2, Supporting Information). Using the tabulated values, band assignments for the GO and FGS shown in Figure 1 can be made as follows: The strong band near 1740 cm^{-1} is assigned to C=O, with possible contributions from acid anhydrides or
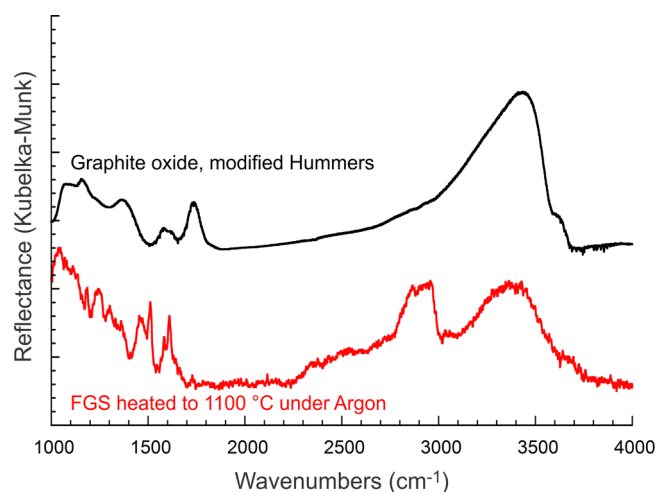
Figure 1. A comparison of the DRIFTS of GO, produced via a modified Hummers technique, to that of FGSs produced by exfoliation (and partial reduction) of the GO and subsequently heated to 1100 °C under argon to further reduce the oxygen content of the FGS to a C/O ~ 100 (see Methods). The subsequent thermal treatment was not at sufficiently high temperature to lower the defect content through annealing; instead, heating at 1100 °C increased the defect content of the heated FGS over that of the GO.[8] The scale of the FGS spectrum has been multiplied by a factor of 100 to improve the visibility of the bands for comparison to that of the GO, resulting in the higher noise level in the FGS spectrum. The strong band between 2800 and 3000 cm^{-1} is related to the aggregation of the sheets on the DRIFTS sample holder. The diffuse reflection spectra are shown in units of reflectance after applying the Kubelka−Munk conversion.[55]

quinones.[9,13,14,18,24] The weak band at 1612 cm^{-1}, a feature occasionally attributed to cyclic ethers,[33] is more often assigned to O−H bending in water molecules physisorbed on the GO,[41] the presence of which has also been used to explain perceived shifts in other functional group absorptions.[29,41−44] A band at 1580 cm^{-1} is attributed to C═C stretches in aromatic regions of the carbon network.[6,9,13,14,18,23] The presence of water[9,18] in the hygroscopic GO[42] is much more apparent as the intense absorption at 3432 cm^{-1}, with the weak shoulder at 3618 cm^{-1} taken as evidence of carboxyl groups.[9,5,18,31,43−45] Hydroxide groups (C−OH) on the GO are indicated by the band centered at 1359 cm^{-1}.

After thermal reduction at 1100 °C under argon, the FGS spectrum shown in Figure 1 exhibits a sharp, intense absorption at 1611 cm^{-1}, possibly indicating the presence of small amounts of physisorbed water between the aggregated sheets of the sample.[42] The C═C aromatic band at 1583 cm^{-1} remains. A broad band between 2800 and 3000 cm^{-1} becomes visible in the spectrum of the heated FGS which does not appear to be related to the spectrum of an isolated sheet. Rather, in studies on similar materials this feature has been attributed to the presence of dimeric carboxylates[46] and associated with interactions between the edges of neighboring graphene oxide sheets. These interactions can be caused by the aggregation of sheets when deposited on the DRIFTS sampling substrate.[47,48] The carbonyl band at 1728 cm^{-1} is almost undetectable in the heated FGS, indicating the loss of carbonyls during high-temperature thermal reduction. The C−OH band (1359 cm^{-1}) in the GO spectrum is not visible in the FGS spectrum, but two new bands at 1512 and 1452 cm^{-1} appear in the spectrum of the FGS. If due to hydroxide groups on the FGS, these are shifted from the tabulated positions, and their presence is

unexpected based on previous descriptions of thermally reduced graphene oxide.[36] In the high-frequency part of the spectrum, the band attributed to carboxyls at 3618 cm^{-1} in the GO spectrum appears to have shifted to 3641 cm^{-1} in the FGS spectrum. Merely extrapolating the assignment of these bands and shifts from previously tabulated values does not explain the apparent shifts and changes in relative intensities, increasing the likelihood of incorrect identification and obscuring the effect of thermally reducing GO to form FGS. Thus, as detailed below, our goal has been to investigate the origin of these variations between GO and FGS through DFT modeling.

As already mentioned, structural models based on DFT have been widely used to obtain insights into the properties and chemical compositions of graphene oxide and its reduced and defective forms.[6,9,30−40] The model structures are then linked to experimental IR spectra by calculating the vibrational spectra of the proposed functional groups.[31−36] These IR calculations typically involve small unit cells and simple cluster models, and the investigated structures include selected functional groups arranged singly or in groups in a fixed manner. In some studies a uniform frequency correction, based on the calculated frequency of vibration of a simple reference molecule,[31,36] is applied to the calculated frequencies that are used to support the experimental band assignments. Problematically, these cluster models do not account for the actual complexity of graphene oxide composition[6,9] and thus may not properly describe the effective interactions between various functional groups and lattice structure (defects and edges) that determine the IR features observed in experiments. Because of the variations in the graphene oxide composition and lattice structure that arise from the different methods used to produce GO and FGSs, more realistic models that integrate functional groups on both sides of the carbon lattice and the lattice defects (including vacancies and edges) are critical for the proper interpretation of the experimental measurements.[30,49−52]

The work presented in this paper demonstrates that experimental IR spectra can be described using first-principles DFT calculations based on graphene oxide models that incorporate oxygen-decorated vacancies and edges. A distinctive feature of our models is that they are constructed using an energetic step-by-step procedure and are further equilibrated thermally by ab initio molecular dynamics (AIMD)[53] simulations. With our modeling approach, we demonstrate that the presence of lattice vacancies or edges intrinsically lead to significant frequency shifts in the OH stretching and bending bands, resulting in absorption bands whose frequencies cannot be explained otherwise and to which no correction needs to be applied. On the other hand, our results also indicate that these frequency shifts are largely unaffected by the presence of water molecules. We further show that carboxyl groups at the edges of fully oxidized graphene contribute unique IR features in the high-frequency OH stretching region, arising from the interplay with neighboring functional groups and the carbon lattice.

■ METHODS

Experiment. The procedure for producing GO using a modified Hummers method[11] has been described previously.[20] FGSs were produced through the simultaneous thermal exfoliation and reduction of graphite oxide as described previously.[6,9,54] Both procedures are summarized in the Supporting Information.

Fourier transform infrared (FTIR) spectra were collected using a modified diffuse reflectance (DR) technique,[55,56] in which the sample (such as GO) was deposited from a suspension onto the surface of a mirror. In a typical procedure, a few milligrams of GO powder were

added to a test tube containing ~2 mL of carbon tetrachloride (Fisher Scientific), shaken, and then agitated using a hand-held probe sonicator (Branson SLPe, Fisher Scientific) for 5 min, all at room temperature, to avoid intercalation or significant adsorption of the CCl_4.[57] An aliquot was removed using a Pasteur pipet and a few (3−4) drops placed on a circular mirror 1 cm in diameter. The CCl_4 evaporated under flowing nitrogen, leaving a thin layer of the sample on the surface. The coated mirror was mounted in the sample holder of a standard DRIFTS accessory (Collector, Barnes Spectra-Tech, Stamford, CT) and placed into the sample chamber of an FTIR spectrometer (Nexus 670 FTIR, Thermo Nicolet, Madison, WI) equipped with a liquid nitrogen-cooled MCT/A detector. Spectra were collected using a slow scan rate (0.16 cm·s^{-1}) at 2 cm^{-1} resolution, and the signal was averaged over 128 scans. No trace amounts of CCl_4 were detectable in the sample after drying nor were the samples heated (save for heating that occurs through sonication). Prior to taking the spectra, the DRIFTS accessory was aligned for maximum signal throughput using an uncoated mirror, which was used to provide the background spectrum. Background and sample measurements were taken only after the sample chamber was sufficiently purged using dry nitrogen to reduce the levels of carbon dioxide and water vapor to barely detectable concentrations in the sampling chamber. The experimental samples were taken from powders dried from suspension and then redispersed in solvent before depositing on the sample holder to dry in place. This procedure resulted in samples composed of a range of multilayer aggregates, varying in size and number of layers and increasing interactions between sheets.

Computational Details. We performed DFT calculations using the QUANTUM ESPRESSO simulation package.[58] We employed the gradient-corrected Perdew−Burke−Ernzerhof (PBE)[59,60] functional for the exchange and correlation energy, norm-conserving pseudopotentials,[61] and a plane wave basis set with kinetic energy cutoff of 80 Ry. AIMD simulations were carried out within the Car−Parrinello framework[53] and the NVT ensemble using a fictitious electron mass of 300 au and a time step of 3 au. A Nosé−Hoover thermostat was chosen to control the ionic temperature with an oscillation frequency of 40 THz.

Extended graphene oxide models were simulated using an orthorhombic cell with a 7.77×8.78 Å in-plane unit cell and a 15 Å periodicity in the direction normal to the carbon plane in order to minimize the interactions between repeated images. For finite graphene oxide sheets, a $30 \times 30 \times 30$ Å cubic cell was used to make sure that no interactions were present between periodic replicas. In all cases, only the Γ point was used to sample k space.

The atomic positions of graphene oxide models were relaxed until the total energy change was less than 0.00014 eV per unit cell and all components of forces were smaller than 0.0025 eV/Å. Vibrational normal frequencies, ω_i, and corresponding eigenvectors, $\{\mathbf{u}_I(\omega_i)\}$,[62] were calculated by diagonalizing the matrix of the interatomic force constants, which were computed as the second derivatives of the system energy with respect to atomic positions via density functional perturbation theory (DFPT).[63] The intensities of IR-active modes were calculated according to

$$I_{IR}(\omega) = \sum_\alpha |\sum_{\beta I} Z_I^{*\alpha\beta} u_I^\beta(\omega)|^2$$

where ω is the phonon frequency, α and β denote the Cartesian components, $Z_I^{*\alpha\beta}$ is the Born effective charge tensor of the Ith ion, and $u_I^\alpha(\omega)$ is the atomic displacement of the Ith ion in the normalized eigenvector of the mode.[63] Details on the calculation of the vibrational density of states are given in the Supporting Information.

RESULTS AND DISCUSSION

As indicated in the descriptions of the spectra shown in Figure 1, the assignment and interpretation of IR spectral features of graphene oxide and its reduced forms still remain somewhat problematic despite the existence of extensive experimental and computational results. IR spectral calculations done using more

sophisticated graphene oxide models that incorporate the different structural features likely to be found on graphene oxide are necessary. We address this by constructing energetic models equilibrated through thermal reduction as described below.

Theoretical Modeling. The computational graphene oxide models used in this study are depicted in Figure 2a−e. An initial
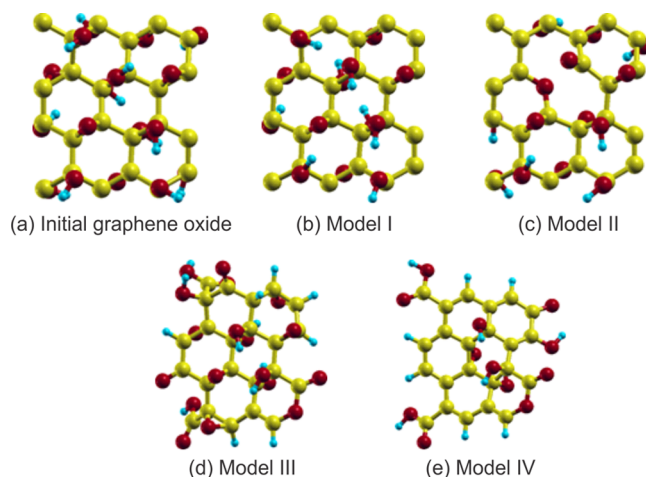

Figure 2. Atomic structures of graphene oxide models. Unit cells of the extended graphene oxide models are displayed in the top panel: (a) Initial graphene oxide with a C/O of ~ 1.4; (b) extended graphene oxide with no lattice defect (Model I); (c) extended graphene oxide with monovacancy (Model II). The full extended graphene oxide models are obtained by periodically repeating the unit cells (a−c). The finite graphene oxide models are depicted in the bottom panel: (d) finite graphene oxide with edges terminated with different functional groups (Model III); (e) simplified version of Model III with fewer functional groups at the edges and on the plane (Model IV).

graphene oxide structure, Figure 2a, was constructed by a systematic step-by-step procedure in which hydroxyls and epoxy groups were successively added in configurations that minimized the total energy of the resulting structure. Neighboring functional groups were generally adsorbed on the different sides of the graphene oxide in order to minimize the stress induced by the adsorption. This initial graphene oxide model contains hydroxyl and epoxy groups on both sides of the plane but no sp^2 carbon bonds in the lattice, and the C/O is ~ 1.4, indicating an almost fully oxidized graphene.

Starting from this structure, extended graphene oxide models were generated by AIMD simulations in which the temperature was gradually increased from 300 to 1200 K at a rate of 50 K per 5 ps. Diffusion and, in some cases, desorption of the functional groups (−OH) were observed during the heating process. Molecular products released from the graphene oxide were removed from the model, and the final structure was further equilibrated at 300 K to confirm its stability. The resulting model (Model I) is shown in Figure 2b. It consists of a periodically repeated unit containing 24 C atoms with 2 C═C double bonds, 8 hydroxyl, and 5 epoxy groups (Figure 3) with a C/O of 1.85.

Another extended graphene oxide model was generated with the same protocol used for Model I but with one C atom removed from the lattice. The resulting structure of graphene oxide containing a monovacancy (Model II) is shown in Figure 2c. The unit cell contains 23 C atoms with 3 C═C double bonds, 8 hydroxyl, 4 epoxy, 1 ketone, and 1 ether groups
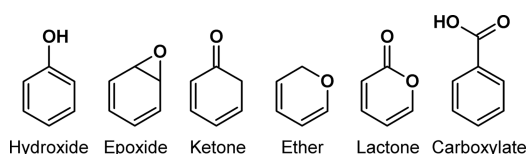
Figure 3. Molecular models of oxygen-containing functional groups thought to exist on GO, graphene oxide, and FGS.

(Figure 3), corresponding to a C/O of 1.64 and a carbon vacancy concentration of about 4%.

As synthesized, graphene oxide sheets are decorated with oxygen-containing functional groups across the plane and on the edges. Hence, we also prepared a finite graphene oxide model by terminating a single unit cell of Model I with hydroxyls, ketone, and carboxyl groups, H atoms, and one lactone group (Figure 3), consistent with recent experimental evidence suggesting that peripheral structures include lactone groups.[5] The hydrogen atom termini were introduced to provide saturation of the edge carbons. The resulting structure (Model III), shown in Figure 2d, has 23 C atoms with no C= C double bond, 5 hydroxyl, 6 epoxy, 2 ketone, 1 lactone, 2 carboxyl groups, and 7 edge-terminating H atoms. The C/O is 1.28, indicating that the carbon lattice is fully oxidized.

Finally, to better understand the effects of the interactions between neighboring functional groups, we considered a simplified version of Model III including 23 C atoms with 7 C=C double bonds, presented in Figure 2e as Model IV, with fewer functional groups at the edges and on the planes: 4 hydroxyl, 1 epoxy, 1 ketone, 1 lactone, 2 carboxyl groups, and 6 edge-terminating H atoms, yielding a structure with a C/O of 1.92.

Extended Graphene Oxide Models—The Vacancy Effect. We first compare the IR spectra of extended graphene oxide Model I, which has no defects in the carbon lattice, and Model II, which contains a vacancy every 24 C atoms, corresponding to a ∼ 4% concentration of monovacancy defects. To determine the vibrational properties, we performed long (41 ps) AIMD simulations at 300 K for both of these models. We selected 18 snapshots at time intervals of 2.3 ps from each MD trajectory, and for each snapshot we optimized the structure and calculated the corresponding infrared spectrum using DFPT.[63] From a normal-mode analysis, we found that the vibrational modes with frequencies below 1000 cm^{-1} correspond to collective motions involving multiple functional groups and the carbon lattice. We thus focus only on the bands above 1000 cm^{-1}, which correspond to vibrational modes that can be assigned to the motions of specific functional groups. The resulting spectra, obtained by averaging over 18 snapshots, are shown in Figure 4a. The contributions of the different snapshots are shown separately in Figure S1, Supporting Information, where the frequency region below 1000 cm^{-1} is also included.

From a normal-mode analysis, we attribute the IR absorption peak at 1664 cm^{-1}, only visible for Model II in Figure 4a, to the stretching of ketone (C=O) groups at vacancy edges. The vibrations of the C=C double bonds in the plane give rise to the IR activities in the region ∼ 1490−1605 cm^{-1}, highlighted by the green bar in Figure 4a. The hydroxyl stretching motions result in the high-frequency bands over 3000 cm^{-1}, while the bending motions contribute to the vibrational bands over-lapping the epoxy stretching modes in the range of ∼ 1250− 1500 cm^{-1}, indicated by the blue bar in Figure 4a. Comparison
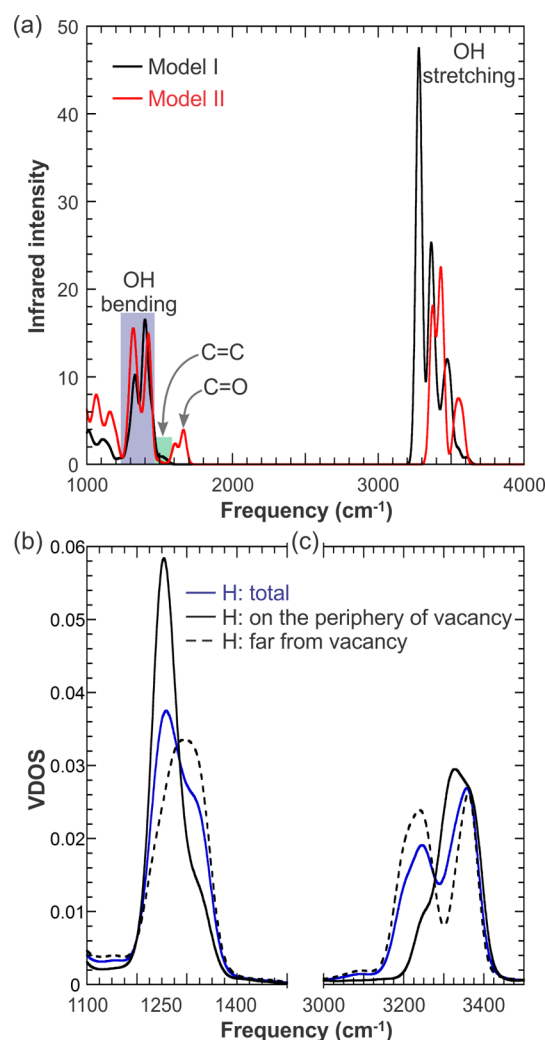

Figure 4. (a) Computed IR spectra of extended graphene oxide models: Model I, with no lattice defect (black), and Model II, with a monovacancy per unit cell (red). The assignment of individual bands is based on a normal-mode analysis. Blue and green bars highlight the overlapping hydroxyl bending and epoxy stretching bands and the C= C double bond bands, respectively. (b) OH bending and (c) OH stretching bands in the VDOS of hydrogen atoms in Model II (graphene oxide with monovacancy) (blue line). Contributions originating from the hydroxyl groups on the periphery of and far from the vacancy are shown as solid and dashed black lines, respectively.

of the calculated vibrational spectra of defect-free and defective graphene oxide shows that the hydroxyl stretching band (3000−4000 cm^{-1}) of defective graphene oxide (Model II) is blue shifted with respect to that of defect-free graphene oxide (Model I). By contrast, the bands in the ∼ 1250−1500 cm^{-1} range of Model II are slightly red shifted in comparison to those of Model I. Although the hydroxyl bending and epoxy stretching bands overlap in this region, analysis of the vibrational density of states (VDOS) of different atomic species (Figure S2, Supporting Information) unambiguously shows that this red shift originates solely from the hydroxyl bending motions. Such shifts indicate a significant influence of vacancy defects on OH vibrations in graphene oxide.

To further characterize the effect of vacancies on OH vibrations, we decomposed the OH bending and stretching modes of Model II into modes contributed by hydroxyl groups

on the periphery of the vacancy and away from it. As shown in Figure 4b, the hydroxyl groups on the periphery of the vacancy indeed exhibit lower bending and higher stretching frequencies in comparison to the hydroxyls far from the vacancy. Such differences can be attributed to the lower physical constraints on the hydroxyl groups located on or near a vacancy. The OH groups on the periphery of the vacancy have fewer opportunities to form hydrogen bonds with neighboring functional groups. This results in more gas-phase-like vibrational motions, demonstrated by stiffer stretching and softer bending modes relative to the hydroxyls far from the vacancy or on defect-free Model I. Further, the size of the vacancy is another factor that may affect the vibrational properties of functional groups in the vicinity of the vacancy.[36] For instance, calculations by Acik et al.[36] show IR frequencies of single ether groups located at divacancies to be red shifted by ~ 55 cm^{-1} relative to the IR frequencies of ethers at monovacancies. Thus, we performed spectral calculations on an extended graphene oxide Model IIb with a divacancy decorated with two ether groups, shown in Figure S3a, Supporting Information. A divacancy in graphene oxide functionalized with two ether groups has been shown to be stable even after high-temperature heat treatment.[15] Comparison of calculated IR spectra for Models II and IIb, reported in Figure S4, Supporting Information, shows that the blue shift of hydroxyl stretching and the red shift of bending frequencies are slightly more pronounced in the IR spectrum of graphene oxide with a divacancy than in that with a monovacancy.

Adsorbed water is known to affect the IR spectra of graphene oxide in both the high-frequency and the fingerprint regions.[31,49,64,65] To obtain (at least qualitative) insight into the influence of water on the vibrational spectra, we performed AIMD simulations in which a water molecule was physisorbed on the extended graphene oxide Models I and II (see Figure S5(a), Supporting Information). Our results show that the interactions between water and graphene oxide contribute to the broadening of the OH stretching band over 3000 cm^{-1} and induce a moderate red shift (~ 130 cm^{-1}) of the hydroxyl stretching frequencies, see Figure S5b, Supporting Information. The hydrogen bonds between water and the hydroxyl groups in graphene oxide facilitate the OH stretching, yielding modes with lower frequencies. We further examined whether water modifies the vacancy-induced vibrational shifts observed in Figure 4 by comparing the spectra of Models I and II, both with an adsorbed water molecule. As shown in Figure S5c, Supporting Information, the vacancy-induced shifts of the hydroxyl stretching and bending bands are essentially unaffected by the presence of adsorbed water.

Finite Graphene Oxide Models—Edge Effects. The IR spectrum of a finite sheet terminated by different functional groups at the edges (Model III) is shown in Figure 5a, where it is compared to the IR spectrum of the extended Model II containing carbon vacancies. Again, only the region above 1000 cm^{-1} is considered. It is evident that there are important differences between the IR spectra of these two models, both in the high-frequency region, $\sim 3000-4000$ cm^{-1}, and in the $\sim 1600-1900$ cm^{-1} range, which correspond mainly to the OH and C=O stretching modes, respectively.

In comparison to the typical OH stretching band at $\sim 3300-3700$ cm^{-1} in the spectrum of the extended Model II, the spectrum of Model III shows two characteristic features (indicated by arrows in Figure 5a) due to the stretching motions of the carboxyl OHs at the edges: a high-frequency
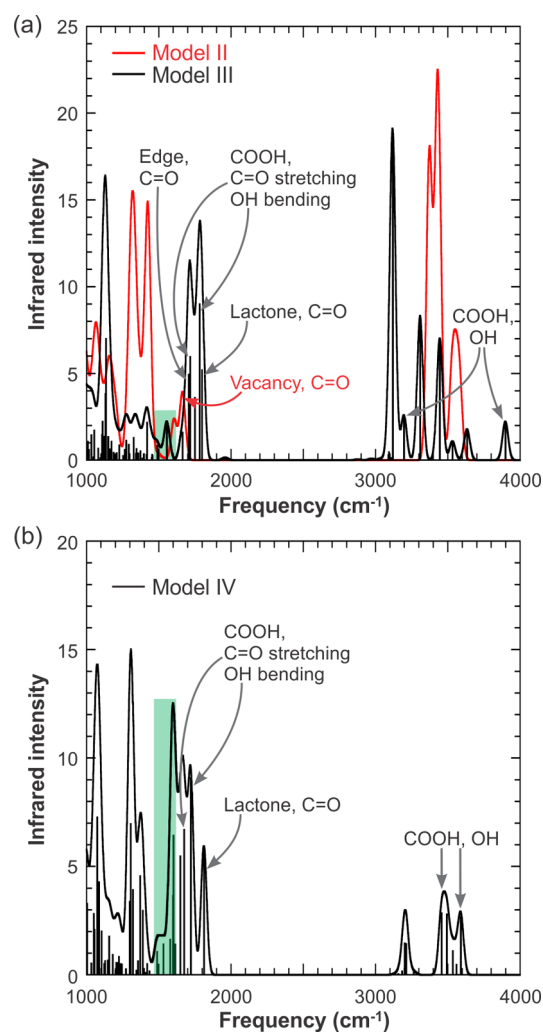

Figure 5. (a) Comparison between the IR spectra of a finite graphene oxide cluster terminated with different functional groups at the edges (Model III, black) and extended graphene oxide with monovacancy (Model II, red). (b) IR spectrum of the simplified graphene oxide cluster Model IV, which contains fewer functional groups at the edges and on the plane. Individual bands are assigned based on a normal-mode analysis. Green bars highlight the region of C=C bands.

mode at ~ 3900 cm^{-1} and a low-frequency one at ~ 3200 cm^{-1} (see also Figure S6a and S6b, Supporting Information). From Figure 5a, it also appears that the hydroxyl vibrations of Model III form a wider band in comparison to the $\sim 3300-3700$ cm^{-1} band of Model II. In the spectrum of Model III, vibrational modes appear around $\sim 3000-3150$ cm^{-1}, caused by the stretching of the C–H bonds at edges. The appearance of this band should not be considered as representative of a true feature of graphene oxide but instead as an artifact of the model.

To elucidate the origin of the low- and high-frequency carboxyl OH stretching modes for Model III, we computed the IR spectrum of Model IV, which has fewer functional groups at the edges and on the plane with respect to Model III. As shown in Figure 5b, the calculated carboxyl OH stretching frequencies of Model IV fall into the range of the normal OH stretching band ($\sim 3300-3700$ cm^{-1}). This suggests that the high- and low-frequency features of carboxyls in Model III are likely to originate from the interactions of the carboxyls with neighboring functional groups and the carbon lattice, which

lead to different orientations of the carboxyl groups with respect to the carbon plane (see Figure S7, Supporting Information) and introduce varying strains in the carboxyl group bonds.

The other interesting range of IR activities in Figure 5a lies in the $\sim 1600-1900$ cm^{-1} range, which corresponds mainly to C=O stretching modes. Four different types of C=O are included in our study: the C=O of lactone and carboxyl groups at sheet edges (Models III and IV) and ketones at sheet edges (Models III and IV) and at vacancies (Model II). From a normal-mode analysis, the vibration at ~ 1800 cm^{-1}, indicated by an arrow in Figure 5a, corresponds to the C=O stretching in a lactone group at a sheet edge (see also Figure S6c, Supporting Information). A combination of carboxyl C=O stretching and OH bending motions at the edges gives rise to the next two modes at frequencies of ~ 1750 and ~ 1780 cm^{-1}, indicated in Figure 5a (see also Figure S6d and S6e, Supporting Information). The stretching motions of ketone groups at edges and vacancies yield IR peaks at ~ 1715 and ~ 1663 cm^{-1}, respectively, which are also indicated in Figure 5a.

Altogether, the frequency shifts of $\sim 50-140$ cm^{-1} that we find for ketone groups embedded in complex environments with respect to an isolated ketone at a vacancy further illustrate the essential effect of the interactions between functional groups on the vibrational properties. As for the OH stretching modes discussed above, the C=O stretching frequencies are thus determined by both the host functional groups and the neighboring groups. This is consistent with calculations presented in earlier work[66] that show that the stretching frequencies of a fixed number (two) of edge ether groups remain essentially unchanged when additional carbon rings are included in the cluster model, whereas an increase of the number of edge ethers from two to seven give rise to large frequency shifts. Besides demonstrating the importance of the interactions between nearby functional groups, these results suggest however that vibrational frequencies calculated using small clusters or simple functionalization may lead to incorrect band assignments for groups on graphene oxide.

On the basis of our calculations, the C=O vibrational frequencies associated with different types of functional groups in the 1600-1900 cm^{-1} range obey the following order: lactone at edge > carboxyl at edge > ketone at edge > ketone at vacancy. This result is consistent with a previous computational study on a decorated graphene cluster,[33] where the following C=O stretching frequencies were predicted: six-membered ring lactone, 1790 cm^{-1}; carboxyl, $\sim 1740-1750$ cm^{-1}; ketone, $\sim 1650-1700$ cm^{-1}. The small, $\sim 10-30$ cm^{-1}, differences between the frequencies obtained in our study and those reported by Fuente et al.[33] for the same functional group can be attributed to the different graphene oxide models, DFT exchange and correlation functionals and basis sets used in the two studies. On the other hand, the calculations reported by Acik et al.[36] for a single functional group on a small carbon cluster gave a higher C=O stretching frequency of carboxyl (1787 cm^{-1}) with respect to lactone (1709 cm^{-1}). Although these frequencies may shift due to the interactions with neighboring functional groups, their relative order is unlikely to change.[33] The discrepancy with our results may be due to the simple cluster model and small unit cell used in the previous work.[36]

We also note that the C=C vibrations of the simplified finite graphene oxide Model IV yield broader and more intense bands than those of extended and finite graphene oxide Models II and

III, highlighted with green bars in Figure 5. The peak of the spectrum within the green region for Model III is mainly attributed to the bending motion between C and edge-terminating H atoms. Such visible differences between the IR bands of C=C vibrations originate from the different number of C=C sp^2 bonds included in the different models. This suggests that the IR signals of the C=C sp^2 bond can serve as an indicator of the presence of sp^2 bonds in graphene oxide and the amount of sp^2 bonds recovered in FGSs, which corresponds to the degree of reduction in experiments.

Finally, we integrate both vacancy and edges in graphene oxide Model IVb (shown in Figure S3b, Supporting Information), which is derived from the finite Model IV by introducing a monovacancy decorated with ketone and ether groups in the middle of the sheet. Comparison between the IR spectra of graphene oxide Models IV and IVb, shown in Figure S8, Supporting Information, shows that the OH stretching mode of the hydroxyl on the periphery of the vacancy has a higher frequency than that of carboxyls and hydroxyls on the defect-free lattice and at edges. This result is thus consistent with our findings that the presence of a vacancy induces a blue shift in the OH stretching band. Vacancy effects on edge carboxyl vibrations are mild, with shifts up to 30 cm^{-1} for both the OH stretching mode and the combined mode of OH bending and C=O stretching. The C=O stretching frequency of the edge lactone group in Model IVb shows a moderate red shift (~ 80 cm^{-1}) with respect to that in Model IV. However, the relative order of the C=O vibrational frequencies of edge lactone and carboxyl is unaffected, with the C=O stretching of the lactone being at higher frequency than that of carboxyl groups.

Comparison between Theory and Experiment—The Role of Vacancies and Edges. Before directly comparing theoretical and experimental spectra, it is useful to assess the accuracy of our theoretical approach in the case of gas-phase molecules. In Table S3, Supporting Information, we compare our calculated harmonic frequencies of gas-phase molecules at the PBE level of theory to experiment. The differences between theory and experiment in Table S3, Supporting Information, are typical of DFT calculations and are not systematic. The IR frequencies of H-involving motions tend to be overestimated by a few wavenumbers in the bending mode and tens of wavenumbers in the stretching modes. On the other hand, frequencies of vibrations between C and O tend to be underestimated by up to ~ 50 cm^{-1}. Due to these different shifts, the frequently used procedure of applying a uniform frequency correction,[36] obtained by comparing the calculated and measured frequencies of a single reference mode, on the computed IR frequencies of different vibrational modes can lead to inaccurate interpretations of spectra and assignments of the various modes. It should also be noted that larger anharmonicity effects should be expected in condensed-phase systems relative to those in the gas phase. We further tested the effect of different supercell sizes on the computed frequencies by considering two graphene oxide models, Models V and VI, containing 24 and 60 carbon lattice sites per unit cell, respectively; see Figure S3c and S3d, Supporting Information. These models comprise the same type of monovacancy decorated with one ketone, one ether, and two hydroxyl groups, yielding a C/O of ~ 6 and ~ 15, respectively. We found that the stretching frequency of the ketone at the monovacancy in Model V is ~ 10 cm^{-1} higher than that in Model VI (see

Figure S9, Supporting Information), indicating that size effects are relatively small.

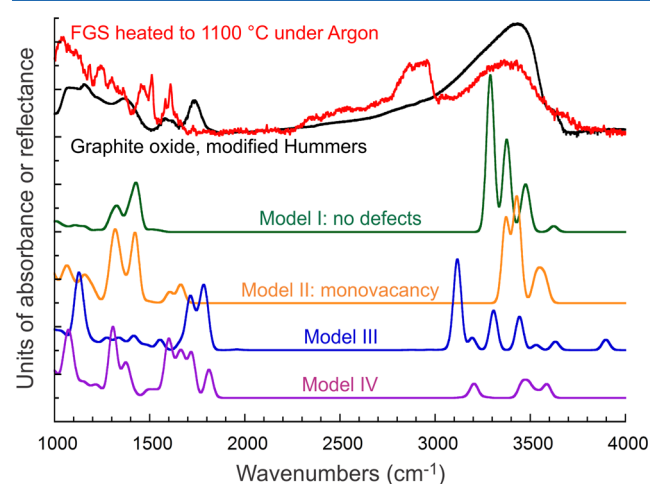Figure 6 shows a comparison of the DRIFTS spectra of GO and FGS already reported in Figure 1 to the calculated

Figure 6. Experimental DRIFTS spectra of GO (black line) and FGS heated to 1100 °C (red line) compared to the calculated IR spectra for Models I−IV. (The FGS spectrum is multiplied by a factor of 100 to enhance visibility.) The FGS was prepared as described in the text to increase the defect content of the carbon lattice while maintaining a detectable level of oxygen-containing functional groups. The strong band between 2800 and 3000 cm^{-1} is related to the aggregation of the sheets on the sample holder. The experimental GO and FGS spectra are shown in Kubelka−Munk units,[55] while the model spectra are shown as units of absorbance. The band centered near 3100 cm^{-1} in the spectrum of Model III arises from C−H stretching on H-terminated edge carbons and is an artifact of the model structure.

absorbance spectra from Models I−IV (also see Table S4, Supporting Information). We recall that the GO is a multilayered stack of graphene oxide sheets, and the FGS, as analyzed, is an aggregation of single sheets; on the other hand, the effect of stacking is not addressed in the theoretical models presented here. Generally, the experimental spectra have closer resemblance to the computed spectrum of Model IV, which includes simple edges and sp^2 carbon bonds, with some resemblance to features that appear in Model II, having a monovacancy defect. The Model I structure, lacking both edges and vacancies, results in an absorption spectrum that bears little resemblance to experimental spectra. This clearly indicates the essential role of the carbon lattice structure (containing defects and edges) on the chemistry of the functional groups. The spectrum of Model III (having no vacancies but incorporating edges), on the other hand, gives insights into the possible structure of fully oxidized graphite, in which the sp^2 carbon−carbon double bonds have been almost completely eliminated and the high number of oxygen-containing functional groups leads to a higher degree of neighbor−neighbor interactions.

As noted earlier, both the hydroscopic GO and the hydrophobic FGS spectra have absorption bands near 1611 cm^{-1}, typically assigned to physisorbed water,[41,48,64,67] with broad bands near 3400 cm^{-1}. The presence of the broad high-frequency band (also indicative of adsorbed water) masks the OH stretching region, but distinct bands attributable to OH bending appear in the GO and FGS spectra below 1550 cm^{-1} (Table S4, Supporting Information). This appears consistent

with the predicted red shift in the OH bending mode in the presence of a vacancy (Model II).

The high-wavelength shoulder (∼ 3670 cm^{-1}) observed in the experimental spectra can be identified with the very high-frequency OH stretching motion of edge carboxyl groups in Model III. Minor contributions may originate from hydroxyl groups in the vicinity of the vacancy. Experimentally, this shoulder may thus provide a useful marker for characterizing the degree of oxidation and number of carboxyl groups in graphene oxide. At lower frequencies, the C=O stretching vibrations give rise to a band in the range of ∼ 1660−1800 cm^{-1} in the computed IR spectrum, while a band with main peak at ∼ 1732 cm^{-1} is observed in the experimental spectra. Our modeling shows that different types of C=O groups, e.g., in lactone or carboxyl at edges, give rise to different vibrational frequencies between ∼ 1660 and 1800 cm^{-1}. This suggests that a shift in the peak position of the C=O band should be observed during the evolution of various C=O groups during the reduction of graphene oxide, as has been shown for multilayered graphene oxide reduced at temperatures below 200 °C.[31] The band position and features correspond more closely to features represented by Models II−IV and are completely absent in Model I. From the computational point of view, this observation alone demonstrates the essential role of edges and vacancies play in the position of the C=O absorption band in the models and in the experimental measurements.

The C=O band so clearly visible in the GO spectrum near 1740 cm^{-1} is much weaker in the spectrum of the FGS heat treated at high temperature, indicating that the loss of oxygen associated with thermal reduction results also in a significant loss of carbonyl C=O groups. We also note that previous studies of oxygen-decorated vacancies and edges show that epoxides are the predominant form of oxygens at vacancies and edges.[15,66] The low oxygen content of the heated FGS is indicated by the 2 orders of magnitude difference in spectral intensity between the GO and the FGS, the latter's spectrum shown in Figures 1 and 6 being multiplied by 100 for easier comparison with the spectrum of the GO.

It is also notable that while the C=O band intensity is much lower in the reduced FGS, the OH bending bands in the reduced FGS are more pronounced, especially ∼ 1460 cm^{-1}. As this frequency is close to that exhibited by OH groups in Model II (∼ 1426 cm^{-1}), the presence of this band is a strong indication that OH groups are closely associated with defects since the defect concentration in the FGS is greater than that in the GO. Interestingly, another intense absorption near 1512 cm^{-1} appears in the FGS spectrum coincident with the appearance of the OH band at ∼ 1452 cm^{-1}. Lying in the C=C region, it is also close to the C−H (edge) absorption of Model II (1555 cm^{-1}). Our models do not allow us to clearly identify the source of this absorption.

The absence of C=C sp^2 bonds in Model III is reflected by the absence of the C=C band in the calculated IR spectra between 1500−1600 cm^{-1}. This band is present in the spectra of Models II and IV and in the measured DRIFTS spectra of the GO and FGS, indicating that sp^2 regions exist in both.

Finally, the broad band between 2800 and 3000 cm^{-1}, more clearly visible in the spectrum of the heated FGS, appears to be related to interactions between sheets,[48] a mode of interaction not modeled in this study.

Comparing calculated and experimental IR spectra provides new insights on the interpretation of spectral features shown

between GO and its thermally reduced form. We attribute the blue shift of the OH stretching band observed in the experimental spectrum of FGS with respect to that of GO to the presence of more lattice vacancies in the reduced FGS. The 1452 cm^{-1} band is more shifted than our models predict, perhaps due to the presence of large vacancies. The band at 1512 cm^{-1} may be related to C−OH present at the sheet edges or on large defects, although we cannot confirm this with our models. The effects of adsorbed water on broadening the OH stretching band lie in not only adding extra OH stretching modes from the water but also shifting the stretching frequencies of hydroxyl groups on graphene oxide. The pronounced blue shifted shoulders in the OH stretching bands, present in both of the experimental spectra shown, originate from the interaction between carboxyl groups and neighboring functional groups. In the fingerprint region, our calculated results indicate a peak shift of the C=O band could be observed during the evolution of various C=O groups during the graphene oxide reduction process due to the change of C=O group species.

CONCLUSIONS

We performed a detailed analysis of the IR vibrational spectra of graphene oxide using first-principles calculations on realistic structural models that include functional groups on both sides of the carbon plane, vacancy defects and edges, and C/O of ∼ 1.3−2. Our results show that vacancy defects and edges have an important influence on the IR signatures of the different functional groups. Specifically, carbon vacancies lead to blue and red shifts of the hydroxyl stretching and bending bands, respectively, in comparison to the OH stretching and bending of defect-free graphene oxide, due to reduced interactions between functional groups around the vacancy. Hydrogen bonds between hydroxyl functional groups and adsorbed water cause a moderate red shift (∼ 130 cm^{-1}) of the hydroxyl stretching frequencies relative to those in the absence of water, but the vacancy-induced shifts of the hydroxyl bands are essentially the same in the absence or the presence of adsorbed water.

We also found that carboxyl groups at the graphene oxide edges can have OH stretching frequencies which are well above and below the typical range, 3300−3700 cm^{-1}, of OH stretching frequencies. Such high (∼ 3900 cm^{-1}) and low (∼ 3200 cm^{-1}) OH stretching frequencies, which originate from the interactions of carboxyl groups at the graphene oxide edges with both neighboring functional groups and the carbon lattice, contribute to the OH stretching band broadening and the high-energy shoulder observed in experiments.

Finally, comparison of the computed and experimental IR spectra provides clear evidence that graphene oxide models including both lattice defects and edges decorated with functional groups are essential for capturing and explaining the spectral features observed in experimental measurements. Importantly, it also suggests that carbon sp^2 regions are present in graphene oxide. These results improve our understanding of the atomic-scale structure of graphene oxide and provide useful insights into the complex interactions of the various functional groups among themselves and with the carbon lattice and may lead to better understanding of the changes that occur in the fabrication of FGS from GO.

ASSOCIATED CONTENT

⑤ Supporting Information

An expanded description of the synthesis of GO and FGS, plus a summary of IR peak assignments from the literature and this work, computed vibrational frequencies for various gas phase molecules, IR spectra for different configuration along AIMD trajectories of **Models I** and **II**, IR spectra of **Models I** and **II** with an adsorbed water molecule, selected vibrational normal modes of **Model III**, and optimized structures of **Models III** and **IV**. The Supporting Information is available free of charge on the ACS Publications website at DOI: 10.1021/acs.jpcc.5b02727.

AUTHOR INFORMATION

Corresponding Author
*Phone: 609-258-3837. E-mail: aselloni@princeton.edu.

Present Address
§Li-Min Liu: Beijing Computational Science Research Center, Beijing 100084, China.

Notes
The authors declare no competing financial interest.

REFERENCES

(1) Loh, K. P.; Bao, Q.; Eda, G.; Chhowalla, M. Graphene oxide as a chemically tunable platform for optical applications. *Nat. Chem.* **2010**, *2*, 1015−1024.

(2) Georgakilas, V.; Otyepka, M.; Bourlinos, A. B.; Chandra, V.; Kim, N.; Kemp, K. C.; Hobza, P.; Zboril, R.; Kim, K. S. Functionalization of graphene: covalent and non-covalent approaches, derivatives and applications. *Chem. Rev.* **2012**, *112*, 6156−6214.

(3) Hwa, T.; Kokufuta, E.; Tanaka, T. Conformation of graphite oxide membranes in solution. *Phys. Rev. A: At., Mol., Opt. Phys.* **1991**, *44*, R2235−R2238.

(4) Kovtyukhova, N. I.; Ollivier, P. J.; Martin, B. R.; Mallouk, T. E.; Chizhik, S. A.; Buzaneva, E. V.; Gorchinskiy, A. D. Layer-by-layer assembly of ultrathin composite films from micron-sized graphite oxide sheets and polycations. *Chem. Mater.* **1999**, *11*, 771−778.

(5) Gao, W.; Alemany, L. B.; Ci, L.; Ajayan, P. M. New insights into the structure and reduction of graphite oxide. *Nat. Chem.* **2009**, *1*, 403−408.

(6) Schniepp, H. C.; Li, J. L.; McAllister, M. J.; Sai, H.; Herrera-Alonso, M.; Adamson, D. H.; Prud'homme, R. K.; Car, R.; Saville, D. A.; Aksay, I. A. Functionalized single graphene sheets derived from splitting graphite oxide. *J. Phys. Chem. B* **2006**, *110*, 8535−8539.

(7) Yan, L.; Punckt, C.; Aksay, I. A.; Mertin, W.; Bacher, G. Local voltage drop in a single functionalized graphene sheet characterized by Kelvin probe force microscopy. *Nano Lett.* **2011**, *11*, 3543−3549.

(8) Punckt, C.; Muckel, F.; Wolff, S.; Aksay, I. A.; Chavarin, C. A.; Bacher, G.; Mertin, W. The effect of degree of reduction on the electrical properties of functionalized graphene sheets. *Appl. Phys. Lett.* **2013**, *102*, 023114−5.

(9) McAllister, M. J.; Li, J. L.; Adamson, D. H.; Schniepp, H. C.; Abdala, A. A.; Liu, J.; Herrera-Alonso, M.; Milius, D. L.; Car, R.; Prud'homme, R. K.; et al. Single sheet functionalized graphene by oxidation and thermal expansion of graphite. *Chem. Mater.* **2007**, *19*, 4396−4404.

(10) Zhu, Y.; Stoller, M. D.; Cai, W.; Velamakanni, A.; Piner, R. D.; Chen, D.; Ruoff, R. S. Exfoliation of graphite oxide in propylene

carbonate and thermal reduction of the resulting graphene oxide platelets. *ACS Nano* **2010**, *4*, 1227−1233.

(11) Marcano, D. C.; Kosynkin, D. V.; Berlin, J. M.; Sinitskii, A.; Sun, Z. Z.; Slesarev, A.; Alemany, L. B.; Lu, W.; Tour, J. M. Improved synthesis of graphene oxide. *ACS Nano* **2010**, *4*, 4806−4814.

(12) Chua, C. K.; Pumera, M. Chemical reduction of graphene oxide: a synthetic chemistry viewpoint. *Chem. Soc. Rev.* **2014**, *43*, 291−312.

(13) Si, Y. C.; Samulski, E. T. Exfoliated graphene separated by platinum nanoparticles. *Chem. Mater.* **2008**, *20*, 6792−6797.

(14) Xu, C.; Wang, X.; Zhu, J. W. Graphene-metal particle nanocomposites. *J. Phys. Chem. C* **2008**, *112*, 19841−19845.

(15) Liu, L.-M.; Car, R.; Selloni, A.; Dabbs, D. M.; Aksay, I. A.; Yetter, R. A. Enhanced thermal decomposition of nitromethane on functionalized graphene sheets: ab initio molecular dynamics simulations. *J. Am. Chem. Soc.* **2012**, *134*, 19011−19016.

(16) Sabourin, J. L.; Dabbs, D. M.; Yetter, R. A.; Dryer, F. L.; Aksay, I. A. Functionalized graphene sheet colloids for enhanced fuel/propellant combustion. *ACS Nano* **2009**, *3*, 3945−3954.

(17) Naebe, M.; Wang, J.; Amini, A.; Khayyam, H.; Hameed, N.; Li, L. H.; Chen, Y.; Fox, B. Mechanical property and structure of covalent functionalised graphene/epoxy nanocomposites *Sci. Rep.* **2014**, *4*, 10.1038/srep04375.

(18) Wei, W.; Qu, X. Extraordinary physical properties of functionalized graphene. *Small* **2012**, *8*, 2138−2151.

(19) Ramanathan, T.; Abdala, A. A.; Stankovich, S.; Dikin, D. A.; Herrera-Alonso, M.; Piner, R. D.; Adamson, D. H.; Schniepp, H. C.; Chen, X.; Ruoff, R. S.; et al. Functionalized graphene sheets for polymer nanocomposites. *Nat. Nanotechnol.* **2008**, *3*, 327−331.

(20) Pope, M. A.; Korkut, S.; Punckt, C.; Aksay, I. A. Supercapacitor electrodes produced through evaporative consolidation of graphene oxide-water-ionic liquid gels. *J. Electrochem. Soc.* **2013**, *160*, A1653−A1660.

(21) Cao, Y. L.; Li, X. L.; Aksay, I. A.; Lemmon, J.; Nie, Z. M.; Yang, Z. G.; Liu, J. Sandwich-type functionalized graphene sheet-sulfur nanocomposite for rechargeable lithium batteries. *Phys. Chem. Chem. Phys.* **2011**, *13*, 7660−7665.

(22) Xiao, J.; Mei, D. H.; Li, X. L.; Xu, W.; Wang, D. Y.; Graff, G. L.; Bennett, W. D.; Nie, Z. M.; Saraf, L. V.; Aksay, I. A.; et al. Hierarchically porous graphene as a lithium-air battery electrode. *Nano Lett.* **2011**, *11*, 5071−5078.

(23) Gao, X.; Li, J.; Guan, D.; Yuan, C. A scalable graphene sulfur composite synthesis for rechargeable lithium batteries with good capacity and excellent columbic efficiency. *ACS Appl. Mater. Interfaces* **2014**, *6*, 4154.

(24) Chabot, V.; Higgins, D.; Yu, A.; Xiao, X.; Chen, Z.; Zhang, J. A review of graphene and graphene oxide sponge: material synthesis and applications to energy and the environment. *Energy Environ. Sci.* **2014**, *7*, 1564−1596.

(25) Dutta, D.; Wood, B. C.; Bhide, S. Y.; Ayappa, K. G.; Narasimhan, S. Enhanced gas adsorption on graphitic substrates via defects and local curvature: a density functional theory study. *J. Phys. Chem. C* **2014**, *118*, 7741−7750.

(26) Wu, Z. Q.; Chen, X. D.; Zhu, S. B.; Zhou, Z. W.; Yao, Y.; Quan, W.; Liu, B. Room temperature methane sensor based on graphene nanosheets/polyaniline nanocomposite thin film. *IEEE Sens. J.* **2013**, *13*, 777−782.

(27) Roy-Mayhew, J. D.; Boschloo, G.; Hagfeldt, A.; Aksay, I. A. Functionalized graphene sheets as a versatile replacement for platinum in dye-sensitized solar cells. *ACS Appl. Mater. Interfaces* **2012**, *4*, 2794−2800.

(28) Kavan, L.; Yum, J.-H.; Graetzel, M. Optically transparent cathode for Co(III/II) mediated dye-sensitized solar cells based on graphene oxide. *ACS Appl. Mater. Interfaces* **2012**, *4*, 6999−7006.

(29) Segal, M. Selling graphene by the ton. *Nat. Nanotechnol.* **2009**, *4*, 612−614.

(30) Kumar, P. V.; Bardhan, N. M.; Tongay, S.; Wu, J.; Belcher, A. M.; Grossman, J. C. Scalable enhancement of graphene oxide properties by thermally driven phase transformation. *Nat. Chem.* **2013**, *6*, 151−158.

(31) Acik, M.; Mattevi, C.; Gong, C.; Lee, G.; Cho, K.; Chhowalla, M.; Chabal, Y. J. The role of intercalated water in multilayered graphene oxide. *ACS Nano* **2010**, *4*, 5861−5868.

(32) Abuelela, A. M.; Farag, R. S.; Mohamed, T. A.; Prezhdo, O. V. Ab initio study of the vibrational signatures for the covalent functionalization of graphene. *J. Phys. Chem. C* **2013**, *117*, 19489−19498.

(33) Fuente, E.; Menéndez, J. A.; Díez, M. A.; Suárez, D.; Montes-Morán, M. A. Infrared spectroscopy of carbon materials: a quantum chemical study of model compounds. *J. Phys. Chem. B* **2003**, *107*, 6350−6359.

(34) Kudin, K. N.; Ozbas, B.; Schniepp, H. C.; Prud'homme, R. K.; Aksay, I. A.; Car, R. Raman spectra of graphite oxide and functionalized graphene sheets. *Nano Lett.* **2008**, *8*, 36−41.

(35) Page, A. J.; Chou, C.-P.; Pham, B. Q.; Witek, H. A.; Irle, S.; Morokuma, K. Quantum chemical investigation of epoxide and ether groups in graphene oxide and their vibrational spectra. *Phys. Chem. Chem. Phys.* **2013**, *15*, 3725−3735.

(36) Acik, M.; Lee, G.; Mattevi, C.; Pirkle, A.; Wallace, R. M.; Chhowalla, M.; Cho, K.; Chabal, Y. The role of oxygen during thermal reduction of graphene oxide studied by infrared absorption spectroscopy. *J. Phys. Chem. C* **2011**, *115*, 19761−19781.

(37) Boukhvalov, D. W.; Katsnelson, M. I. Modeling of graphite oxide. *J. Am. Chem. Soc.* **2008**, *130*, 10697−10701.

(38) Carlsson, J. M.; Hanke, F.; Linic, S.; Scheffler, M. Two-step mechanism for low-temperature oxidation of vacancies in graphene. *Phys. Rev. Lett.* **2009**, *102*, 166104.

(39) Yan, J.-A.; Xian, L.; Chou, M. Y. Structural and electronic properties of oxidized graphene. *Phys. Rev. Lett.* **2009**, *103*, 086802.

(40) Zhou, S.; Bongiorno, A. Density functional theory modeling of multilayer "epitaxial" graphene oxide. *Acc. Chem. Res.* **2014**, *47*, 3331−3339.

(41) Szabo, T.; Berkesi, O.; Forgo, P.; Josepovits, K.; Sanakis, Y.; Petridis, D.; Dekany, I. Evolution of surface functional groups in a series of progressively oxidized graphite oxides. *Chem. Mater.* **2006**, *18*, 2740−2749.

(42) Lerf, A.; He, H. Y.; Forster, M.; Klinowski, J. Structure of graphite oxide revisited. *J. Phys. Chem. B* **1998**, *102*, 4477−4482.

(43) Dreyer, D. R.; Park, S.; Bielawski, C. W.; Ruoff, R. S. The chemistry of graphene oxide. *Chem. Soc. Rev.* **2010**, *39*, 228−240.

(44) Gao, X.; Jang, J.; Nagase, S. Hydrazine and thermal reduction of graphene oxide: reaction mechanisms, product structures, and reaction design. *J. Phys. Chem. C* **2010**, *114*, 832−842.

(45) Jung, I.; Field, D. A.; Clark, N. J.; Zhu, Y. W.; Yang, D. X.; Piner, R. D.; Stankovich, S.; Dikin, D. A.; Geisler, H.; Ventrice, C. A.; et al. Reduction kinetics of graphene oxide determined by electrical transport measurements and temperature programmed desorption. *J. Phys. Chem. C* **2009**, *113*, 18480−18486.

(46) Shipman, S. T.; Douglass, P. C.; Yoo, H. S.; Hinkle, C. E.; Mierzejewski, E. L.; Pate, B. H. Vibrational dynamics of carboxylic acid dimers in gas and dilute solution. *Phys. Chem. Chem. Phys.* **2007**, *9*, 4572−4586.

(47) Jeon, I.-Y.; Shin, Y.-R.; Sohn, G.-J.; Choi, H.-J.; Bae, S.-Y.; Mahmood, J.; Jung, S.-M.; Seo, J.-M.; Kim, M.-J.; Wook Chang, D.; et al. Edge-carboxylated graphene nanosheets via ball milling. *Proc. Natl. Acad. Sci. U. S. A.* **2012**, *109*, 5588−5593.

(48) Szabó, T.; Berkesi, O.; Dékány, I. DRIFT study of deuterium-exchanged graphite oxide. *Carbon* **2005**, *43*, 3186−3189.

(49) Kim, S.; Zhou, S.; Hu, Y.; Acik, M.; Chabal, Y. J.; Berger, C.; de Heer, W.; Bongiorno, A.; Riedo, E. Room-temperature metastability of multilayer graphene oxide films. *Nat. Mater.* **2012**, *11*, 544−549.

(50) Kumar, P. V.; Bernardi, M.; Grossman, J. C. The impact of functionalization on the stability, work function, and photoluminescence of reduced graphene oxide. *ACS Nano* **2013**, *7*, 1638−1645.

(51) Bagri, A.; Mattevi, C.; Acik, M.; Chabal, Y. J.; Chhowalla, M.; Shenoy, V. B. Structural evolution during the reduction of chemically derived graphene oxide. *Nat. Chem.* **2010**, *2*, 581−587.

(52) Paci, J. T.; Belytschko, T.; Schatz, G. C. Computational studies of the structure, behavior upon heating, and mechanical properties of graphite oxide. *J. Phys. Chem. C* **2007**, *111*, 18099−18111.

(53) Car, R.; Parrinello, M. Unified approach for molecular dynamics and density-functional theory. *Phys. Rev. Lett.* **1985**, *55*, 2471−2474.

(54) Hsieh, A. G.; Korkut, S.; Punckt, C.; Aksay, I. A. Dispersion stability of functionalized graphene in aqueous sodium dodecyl sulfate solutions. *Langmuir* **2013**, *29*, 14831−14838.

(55) Venter, J. J.; Vannice, M. A. A diffuse reflectance FTIR spectroscopic (DRIFTS) investigation of carbon-supported metal-carbonyl clusters. *J. Am. Chem. Soc.* **1987**, *109*, 6204−6205.

(56) Venter, J. J.; Vannice, M. A. Applicability of DRIFTS for the characterization of carbon-supported metal-catalysts and carbon surfaces. *Carbon* **1988**, *26*, 889−902.

(57) Barroso-Bujans, F.; Cerveny, S.; Verdejo, R.; del Val, J. J.; Alberdi, J. M.; Alegria, A.; Colmenero, J. Permanent adsorption of organic solvents in graphite oxide and its effect on the thermal exfoliation. *Carbon* **2010**, *48*, 1079−1087.

(58) Giannozzi, P.; Baroni, S.; Bonini, N.; Calandra, M.; Car, R.; Cavazzoni, C.; Ceresoli, D.; Chiarotti, G. L.; Cococcioni, M.; Dabo, I. QUANTUM ESPRESSO: a modular and open-source software project for quantum simulations of materials. *J. Phys.: Condens. Matter* **2009**, *21*, 395502.

(59) Perdew, J. P.; Burke, K.; Ernzerhof, M. Generalized gradient approximation made simple. *Phys. Rev. Lett.* **1996**, *77*, 3865−3868.

(60) Perdew, J. P.; Burke, K.; Ernzerhof, M. Generalized gradient approximation made simple [Phys. Rev. Lett. 77, 3865 (1996)]. *Phys. Rev. Lett.* **1997**, *78*, 1396−1396.

(61) http://www.quantum-espresso.org/pseudopotentials/ (accessed July 20, 2015).

(62) Wen, X.; Garland, C. W.; Hwa, T.; Kardar, M.; Kokufuta, E.; Li, Y.; Orkisz, M.; Tanaka, T. Crumpled and collapsed conformations in graphite oxide membranes. *Nature* **1992**, *355*, 426−428.

(63) Baroni, S.; de Gironcoli, S.; Dal Corso, A.; Giannozzi, P. Phonons and related crystal properties from density-functional perturbation theory. *Rev. Mod. Phys.* **2001**, *73*, 515−562.

(64) Dimiev, A. M.; Alemany, L. B.; Tour, J. M. Graphene oxide. origin of acidity, its instability in water, and a new dynamic structural model. *ACS Nano* **2013**, *7*, 576−588.

(65) Acik, M.; Carretero-González, J.; Castillo-Martínez, E.; Rogers, D. M.; Guzman, R.; Baughman, R. H.; Chabal, Y. J. Reconstructed ribbon edges in thermally reduced graphene nanoribbons. *J. Phys. Chem. C* **2012**, *116*, 24006−24015.

(66) Acik, M.; Lee, G.; Mattevi, C.; Chhowalla, M.; Cho, K.; Chabal, Y. J. Unusual infrared-absorption mechanism in thermally reduced graphene oxide. *Nat. Mater.* **2010**, *9*, 840−845.

(67) Eigler, S.; Enzelberger-Heim, M.; Grimm, S.; Hofmann, P.; Kroener, W.; Geworski, A.; Dotzer, C.; Röckert, M.; Xiao, J.; Papp, C.; et al. Wet chemical synthesis of graphene. *Adv. Mater.* **2013**, *25*, 3583−3587.

(68) Larciprete, R.; Fabris, S.; Sun, T.; Lacovig, P.; Baraldi, A.; Lizzit, S. Dual path mechanism in the thermal reduction of graphene oxide. *J. Am. Chem. Soc.* **2011**, *133*, 17315−17321.